EuroSun2026

# STATE OF CHARGE DETERMINATION OF AN ICE STORAGE FOR BUILDING APPLICATIONS

Gayaneh Issayan, Bernhard Zettl, Christian Wagner, Matthias Brunhuber, Emel Mehmedovski

*University of Applied Sciences Upper Austria, Energy Research Group ASIC, Wels, Austria*

*Gayaneh.Issayan@fh-wels.at*

**Summary**

Ice storage systems represent an attractive technology for thermal energy storage in both cooling and heating applications. Efficient operation control requires reliable information on the state of charge (SOC), which remains challenging under practical operating conditions. This work presents the development and validation of a low-cost capacitive sensor for SOC monitoring based on resonance frequency changes caused by ice formation around a heat exchanger. The sensor was implemented in a 1.25 $m^3$ ice storage system and evaluated during multiple charging and discharging cycles under real operating conditions. The measured frequency signal was compared with a commercial reference sensor and showed a good correlation over a wide range of ice fractions during both ice growth and melting. The signal processing enabled reliable tracking of the storage state. Owing to its simple design and low manufacturing cost, the sensor offers the potential for distributed measurements using multiple sensing locations within a single storage tank, providing improved information on the spatial ice distribution. By combining the measured capacitance changes with the geometry of the heat exchanger and storage system, a thermal SOC concept analogous to that used for electrochemical batteries can be established. The results demonstrate that capacitive sensing is a robust, scalable, and economically attractive approach for SOC determination and advanced operation control of ice storage systems.

*Ice storage, state of the charge (SOC), capacitive sensor, operation control*

*Field of application for the findings: Thermal energy storage*

*Addressed audience: Researchers and academics, industrial stakeholders*

## 1. Introduction

The increasing integration of renewable energy technologies into residential and commercial buildings requires energy storage solutions capable of balancing temporal mismatches between energy generation and demand. In this context, ice storage systems have emerged as promising thermal energy storage (TES) technologies for both heating and cooling applications (Vivian et al., 2023). Their flexibility enables efficient integration with heat pumps, solar thermal collectors, and other renewable energy technologies, facilitating load shifting and improving the overall performance of building energy systems (Mancin and Noro, 2020; Carbonell et al., 2016). As latent TES, they utilize the phase transition between water and ice to store and release large amounts of thermal energy within a narrow temperature range. Compared to sensible TES systems, such as conventional hot-water tanks, latent TES offer substantially higher energy storage densities. During the phase transition of water at 0 °C, approximately 334 $kJ\,kg^{-1}$ of latent heat are absorbed or released. This energy corresponds roughly to the amount required to heat one kilogram of water from 0 °C to 80 °C (Li et al., 2023). Furthermore, water is an attractive phase-change material phase change material (PCM) due to its low cost, non-toxicity, widespread availability, and high latent heat (Vivian et al., 2023). Additionally, the straightforward integration of water-based ice storage systems into existing hydraulic circuits contributes to their attractiveness as a sustainable and economically viable solution for building energy applications. Despite these advantages, several technical challenges continue to limit the broader deployment of ice storage technology.

The development of efficient heat exchanger (HEX) configurations, the detailed understanding of system-specific phase-change processes during charging and discharging, particularly under partial cycling conditions, and the accurate quantification of the storage state of charge (SOC) remain subjects of ongoing research to unlock the full potential of ice storges. Reliable SOC determination is notably important, as it directly affects system control, operational optimization, energy management strategies, and long-term performance assessment(Colangelo et al., 2020). For sensible TES, the SOC can often be estimated directly from temperature measurements because the stored energy is strongly correlated with the storage medium temperature. In latent TES, however, the presence of both liquid and solid phases during the phase transition with complicates this approach. Since the PCM temperature remains nearly constant during freezing and melting, temperature measurements alone provide only limited information about the actual amount of energy stored. SOC determination therefore requires additional information regarding the distribution and proportion of liquid and solid phases within the storage. Numerous methods for SOC determination in latent TES have been proposed. Comprehensive reviews have categorized SOC estimation techniques according to local and global measurement principles and discussed their respective advantages and limitations (Zsembinszki et al., 2020). A commonly applied approach is the integration of charging and discharging energy flows through the HEX (Zsembinszki et al., 2020). Although conceptually straightforward, its accuracy depends heavily on the estimation of thermal losses, leading to error accumulation during long-term operation. Steinmaurer et al. (Steinmaurer et al., 2014) investigated pressure-based methods that exploit the volumetric expansion of water during freezing. Other researchers have proposed conductivity-based approaches that utilize the large difference in electrical conductivity between liquid water and ice. Ezan et al. (Ezan et al., 2011) demonstrated that the latter methods can achieve good agreement with image-based reference measurements. Among the available techniques, capacitive sensing represents a particularly promising approach due to its simplicity, low hardware requirements, and direct relationship to the phase composition within the ice storage. The method exploits the significant difference in dielectric properties between water and ice. Owing to their distinct dielectric relaxation behavior, the relative permittivities of the two phases differ substantially at higher excitation frequencies, enabling the detection of phase transitions and the estimation of ice-layer growth through capacitance measurements (Artemov and Volkov, 2014; Volkov and Vasin, 2019; Dou et al., 2009). Previous studies have successfully applied capacitive sensing for ice detection and ice-thickness monitoring under controlled conditions (Artemov and Volkov, 2014; Dou et al., 2009; Wagner and Issayan, 2025). Compared to optical methods, capacitive sensors do not require visual access to the storage volume and can therefore be integrated directly into practical systems. Furthermore, unlike energy-balance-based methods, the measured signal is directly linked to the local phase state and is not affected by cumulative integration errors. However, investigations on large-scale domestic ice storage systems and complex HEX geometries remain limited, leaving open questions regarding measurement accuracy, robustness, and practical applicability. The present work addresses this research gap through a comprehensive experimental investigation of SOC determination methods using an upscaled domestic ice storage system equipped with a spiral HEX and an in-house developed capacitive sensor.

In contrast to our previous work (Wagner and Issayan, 2025; Issayan et al., 2025), which focused on numerical modeling and experimental analysis of ice layer formation and validation of a commercial capacitive sensor, the present study is exclusively dedicated to validation of the newly developed sensor in realistic storage operation. The developed sensor is low-cost, easy-to-manufacture and can be adapted to different HEX geometries without modification of the HEX itself, as it is flexibly installed alongside the HEX surface. The objective is not to achieve highly precise local ice-thickness measurements but rather to obtain robust and reproducible information about the charging state of the storage. The results provide valuable insights into the applicability, accuracy, and limitations of capacitive SOC determination method and contribute to the development of reliable and cost-effective monitoring strategies for future building-integrated ice storage systems.

## 2. Experimental Setup

The experimental methodology employed in this work includes a detailed description of the ice-storage system, the construction and measurement principle of the developed capacitive sensor, as well as the experimental procedures used for performance evaluation and validation against a commercial reference sensor. Data acquisition was performed using an ALMEMO data logger (Ahlborn), with measurements recorded at intervals of 30 s or 60 s depending on the experiment. The sensors were connected via corresponding ALMEMO connectors equipped with the required signal conditioning and electronic interfaces. All data processing, filtering, and statistical analyses were carried out in MATLAB.

## *2.1 Ice Storage*

The experimental investigations were conducted using a ice storage system presented in Figure 1 and consisting of a cylindrical stainless-steel tank equipped with six spirally wound stainless-steel HEX units, denoted as registers $R1$–$R5$. The uppermost register was excluded from operation and used for sensor installation, as surface effects near the free water level may influence the local thermal conditions and result in behavior that is not representative of the bulk ice storage volume. Each register contains four parallel channels for the heat-transfer fluid (HTF). The HTF is a 50 wt.% aqueous triethylene glycol (TEG) solution, enabling operation at sub-zero temperatures without freezing. The storage tank holds approximately 1250 liters of water, while the HEX registers provide an internal volume of 63 liters and a total heat-transfer surface area of 14 $m^2$. The vertical spacing between adjacent registers is approximately 110 mm. A three-dimensional representation of the storage tank and the arrangement of the HEX registers is shown in Figure 1a. To monitor the thermal behavior of the storage, the tank was instrumented with 17 temperature sensors distributed across different vertical and radial positions. In addition, two capacitive sensors were installed: a reference sensor C1 shown by the violet dashed rectangle in Figure 1b and the newly developed capacitance-based sensor also indicated by the green dashed rectangle C2 in Figure 1b. The reference sensor purchased from HB Products detects ice-thickness and was mounted parallel to the a HEX registers surface. The sensor is designed to monitor ice-layer growth on straight pipes up to a thickness of 50 mm which is converted to %. Using the manufacturer's calibration software, the sensor output was converted into a state-of-charge (SOC) value, representing the percentage of the sensor length covered by ice. The complete list of sensor arrangement and measurement locations are summarized in Table 1.

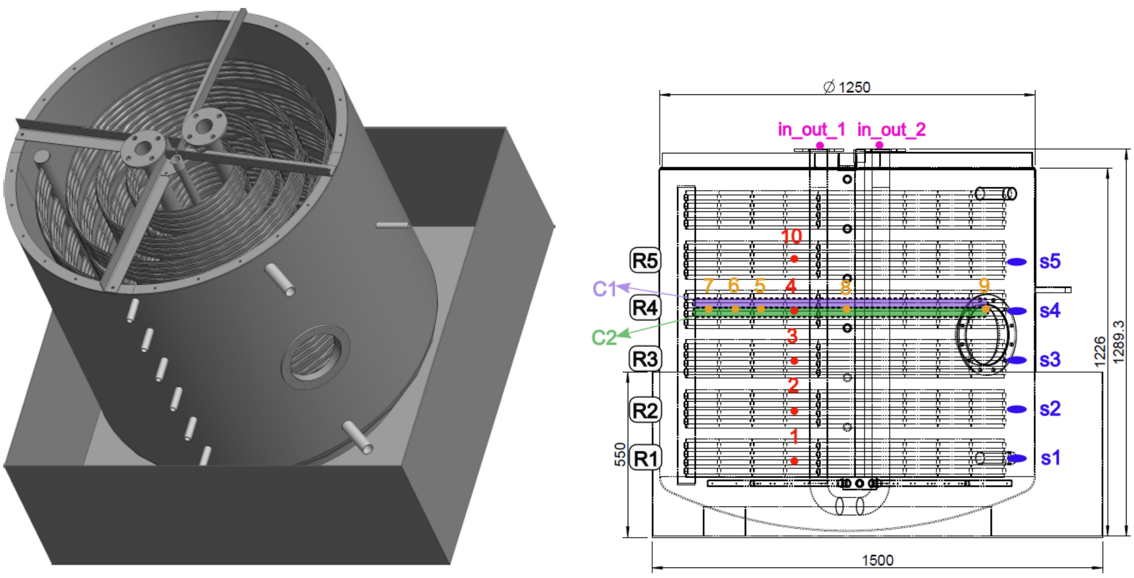


**(a)** 3D representation of the storage.

**(b)** Sensor placement.

**Fig. 1:** Ice storage setup: (a) 3D drawing of the ice storage with a top view of the spiral steel HEX register. In and output HEX fluid pipes are also shown in the middle of the storage (©ECOTHERM Austria GmbH, Christof Lehner). (b) Schematic overview of sensor placement in the tank (see Table 1).

**Tab. 1:** List of main sensors utilized for the determination of state of the charge of the storage.

| Sensor Type | Position | Name | Aim |
|---|---|---|---|
| Temperature | R1 - R5 | T1 - T4, T10 | vertical (depth) |
| Temperature | R4 | T4 - T9 | horizontal (radial) |
| Temperature | R1 - R5 | Tin-out-1 & Tin-out-2 | HTF temeprature in/output |
| Temperature | - | Ts1 - Ts5 | immersion sensors outer shell |
| Capacitive | R4 | C1 | ice layer thickness (commercial) |
| Capacitive | R4 | C2 | ice layer thickness (self-built) |
| Flowmeter | - | F | flow rate of HTF |

The hydraulic configuration of the experimental setup is illustrated in Figure 2. A process thermostat providing a nominal cooling capacity of 24 kW was connected to the laboratory hydraulic ring circuit via the HEX $W2101$ and circulation pump $P2101$. The secondary test circuit comprised an additional HEX $W2102$, circulation pump $P2301$, and the ice storage unit. The thermal power transferred to the storage was determined using a power measurement unit installed upstream of the storage. Between those circuits the temperature is measured by $T2105$ and $T2104$. The main thermal measurement is based on the inlet temperature $T_{\mathrm{in}}$, outlet temperature $T_{\mathrm{out}}$, and the volumetric flow rate of the HTF. This arrangement enabled continuous monitoring of the charging and discharging processes as well as the thermal state of the storage throughout the experiments. Since this study focuses on SOC determination using a capacitive sensing approach, a comprehensive analysis of the thermodynamic performance and energy efficiency of the ice storage system is beyond the scope of the present work.

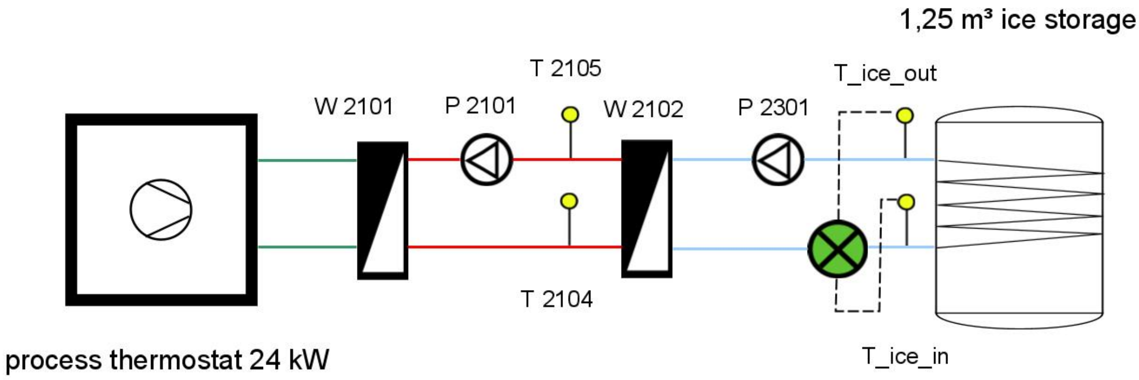


**Fig. 2:** Hydraulic scheme of the experimental setup showing the primary cooling loop, secondary heat transfer fluid circuit, ice storage unit, circulation pumps, HEXs, and thermal power measurement system (©Harald Dehner, FHOOE).

### *2.2 Capacitive Sensor*

The developed capacitance sensor is based on the multivibrator circuit shown in Figure 3. For clarity, the circuit can be divided into three functional sections, highlighted in different colors.

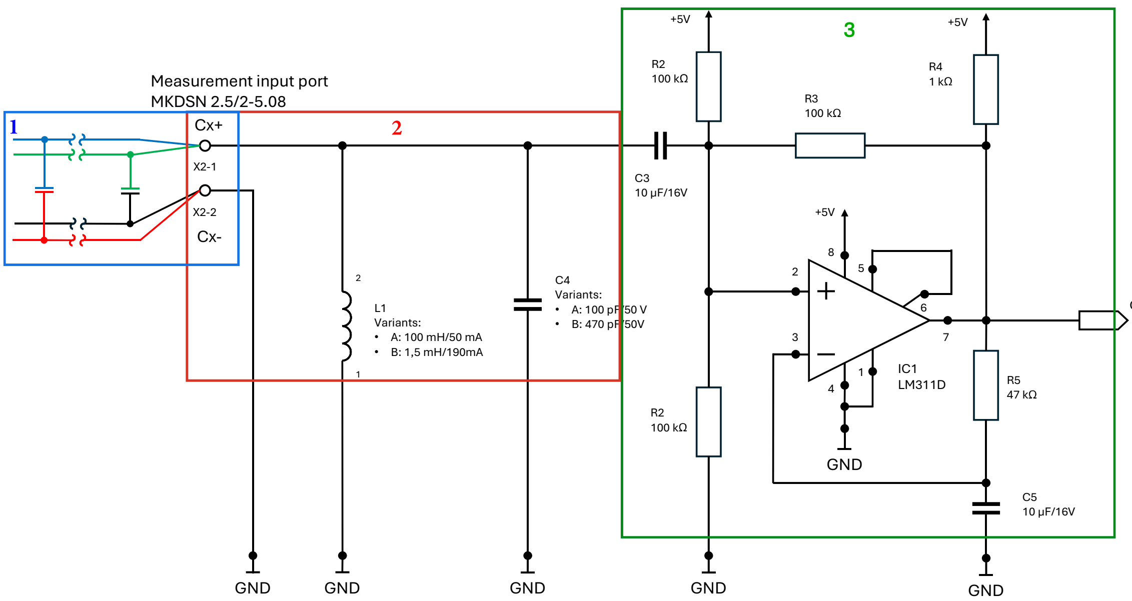


**Fig. 3:** Capacitance sensor: (1) blue four-wire cable is the sensing unit. (2) red is the LC resonant circuit. (3) green is the relaxation oscillator and signal-conditioning unit.

The first section, indicated by the blue rectangle (1), represents the sensing element. It consists of a four-wire cable arrangement that acts as the capacitive measuring element. The sensor was installed parallel to a reference sensor along the HEX, maintaining the same measurement range and distance from the ice thickness (0–50 mm). Variations in the surrounding dielectric properties alter the effective capacitance of the cable arrangement, thereby influencing the resonant behavior of the circuit. The second section, highlighted by the red rectangle (2), forms the resonant circuit. This section consists of a parallel LC resonator, where the sensor capacitance acts as the variable capacitive element. The resonator generates an oscillating voltage whose resonance frequency is determined by the inductance and capacitance according to $f_{\text{res}} = \frac{1}{2\pi\sqrt{LC}}$.

Changes in the sensor capacitance therefore directly result in a shift of the resonance frequency. Depending on the selected components, two operating frequency ranges are available, with approximately 50 kHz and 190 kHz resonance frequency, respectively. The latter was used in this work, as it has shown a better signal-to-noise-ratio. The third section, shown by the green rectangle (3), implements a relaxation oscillator and signal-conditioning stage. As illustrated, this section can be subdivided into several functional circuits. The oscillator contains two feedback loops. At the input, a high-pass filter suppresses low-frequency disturbances and offsets, while a voltage divider network defines the switching thresholds of the Schmitt trigger through positive (non-inverting) feedback. The resistors $R_1$, $R_2$, and $R_3$ determine the upper and lower threshold voltages and therefore the hysteresis characteristics of the Schmitt trigger. The primary purpose of the relaxation oscillator is to generate a continuous self-sustained oscillation without the need for an external excitation source. The resonance signal originating from the LC tank circuit is converted into a stable square-wave output signal whose frequency corresponds directly to the resonance frequency of the sensing circuit. Consequently, variations in capacitance are transformed into frequency changes, enabling a robust and noise-resistant frequency-based measurement principle. The final sensor output is therefore a digital square-wave signal that can be measured with a microcontroller or frequency counter. Since the measured quantity is encoded in the signal frequency rather than its amplitude, the sensor is comparatively insensitive to signal attenuation, voltage fluctuations, and electromagnetic interference.

## 3. Results and Discussion

Similar to the SOC concept used for electrical batteries, the sensor is intended to provide a indication of the available storage capacity and the progression of the charging process. For practical operation, reproducibility and robustness are therefore considered more important than absolute measurement accuracy. The investigated ice storage system can only be charged until approximately 80% of the water volume has been frozen. Beyond this limit, continued ice growth may generate excessive mechanical stresses on the storage walls and internal components due to volumetric expansion during freezing. The capacitive sensor is intended to detect the formation and growth of the ice layers and, in particular, identify the point at which adjacent ice layers begin to merge. Once the HEX surfaces are completely covered with ice and the ice fronts growing from neighboring HEX registers start to connect in the center of the storage volume, further charging becomes increasingly ineffective from an energetic perspective. At this stage, heat transfer is significantly reduced due to the additional thermal resistance of the ice layer, while the risk of mechanical loading increases. Consequently, the sensor can be used as an operational tool to determine an appropriate charging endpoint and prevent unnecessary energy consumption and excessive ice accumulation.

To evaluate the performance of the developed capacitance sensor, multiple charging and discharging cycles of the ice storage were conducted. Depending on the initial thermal state of the storage, a complete charging process typically required three to four days. Charging (freezing) was generally performed during working hours (approximately 8–10 h per day), while the process thermostat was switched off during nights and weekends. To minimize thermal losses during these periods, the top of the storage tank was additionally insulated, resulting in a noticeable reduction of ice losses. The following section focuses on the thermal behavior of the storage and the response of the implemented sensing system. In particular, the temperature measurements and the frequency-based capacitance sensor signals are compared with the reference sensor to check for correlation and calibration.

Figure 4 presents selected temperature measurements together with the reference sensor signal. A characteristic feature of the cooling process is the water density anomaly around 4 °C. This effect is particularly evident in the temperature sensors $T_1$ (yellow dotted line) and $T_{10}$ (violet dashed line), which are located at the greatest

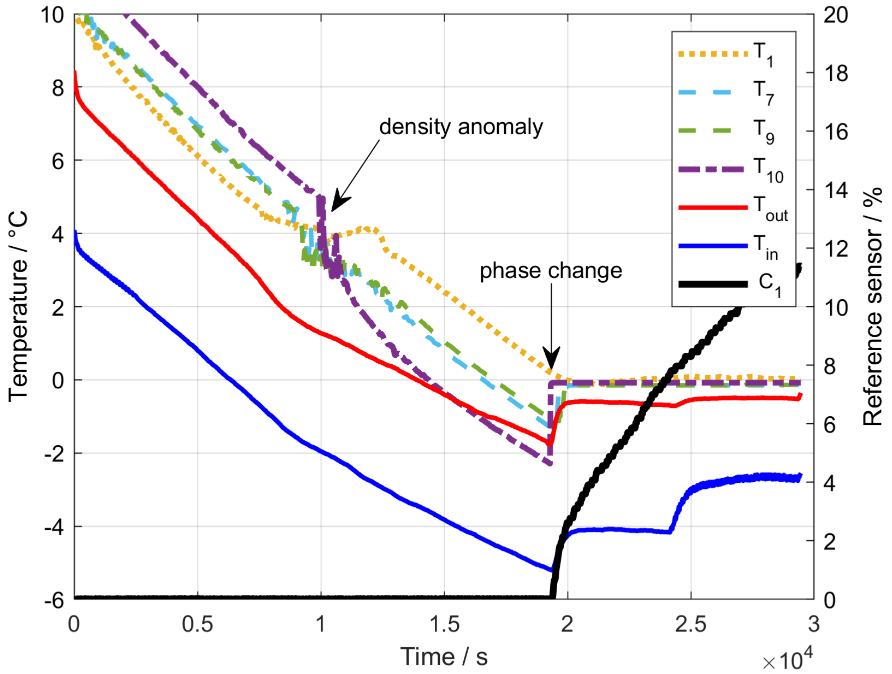


**Fig. 4:** Selected temperature measurements $T_1 - -T_{10}$, as well as $T_{in}$ and $T_{out}$ and the corresponding reference sensor signal $C_1$. The data reveal the characteristic water density anomaly near 4 °C (temperature of maximum density) as well as the phase transition during freezing, both of which are clearly identifiable in the measured sensor response (see black arrows).

vertical distance from one another. During the anomaly, the temperature profiles of these two sensors reverse their order, reflecting the density-driven stratification and redistribution of water within the tank. In contrast, sensors $T_7$ and $T_9$ are located approximately on the same horizontal layer and therefore experience nearly identical thermal conditions. As a result, no pronounced anomaly-related behavior can be observed in their respective temperature profiles. The onset of the phase change can be identified from the distinct step in the reference sensor signal (thick black line). Simultaneously, a sharp temperature increase is observed in $T_{10}$, which is located in the upper and second-coldest layer of the storage tank. A similar but less pronounced step is subsequently visible in $T_7$ and $T_9$. In contrast, sensors located in regions with nearly uniform thermal conditions show little or no discontinuity in their temperature profiles. At the same time, the solid blue and red curves exhibit a distinct step followed by an extended plateau, indicating the release of latent heat during the phase transition. Shortly thereafter, a second step becomes visible, suggesting the progression of the phase-change front into another region of the storage tank and indicating that the phase transition proceeds in multiple stages rather than uniformly throughout the entire volume.

The measured data points in Figure 5 exhibit a considerable spread, resulting in an adequate coefficient of determination in the first case and relatively low one for the second series ($R^2 \approx 0.89$ and 0.7). However, both sensors show a comparable overall response. After offset subtraction (detrending), the frequency signal of the developed sensor covers a range of approximately 0–600 Hz, corresponding to the a measurement range of 0–50 % for reference sensor. The observed scatter indicates a significant level of measurement noise, which led to the use of a Butterworth filtering approach. The filtered data were subsequently evaluated to assess whether the underlying sensor signal still contains a meaningful correlation with the reference measurement despite the high noise level.

The filtered sensor signals (solid blue lines) are shown in Figure 6 together with the corresponding raw data. The Butterworth filter effectively suppresses the high-frequency noise while preserving the overall trend of the measurement. As a result, the correlation between the developed capacitance sensor and the reference sensor becomes significantly more apparent. In the first case (Figure 6a), the noise level increases with increasing ice thickness, whereas in the second case (Figure 6b) the noise amplitude remains relatively constant throughout the measurement period. Despite these differences, the filtered signals clearly reproduce the behavior of the reference sensor, indicating that the capacitance sensor provides meaningful information on the freezing and melting processes within the storage.

To further evaluate the performance of the developed sensor, additional charging data were analyzed. Similar

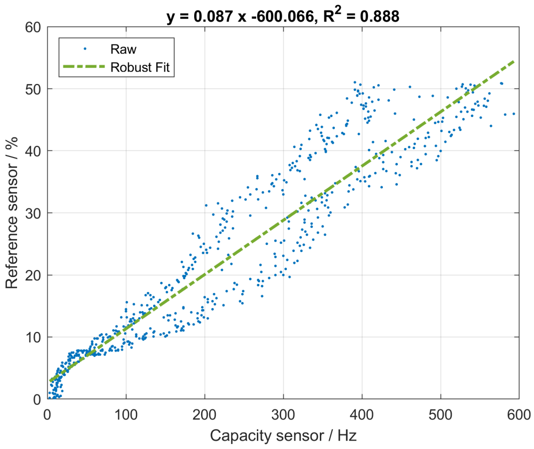


**(a)** First measurement cycle.

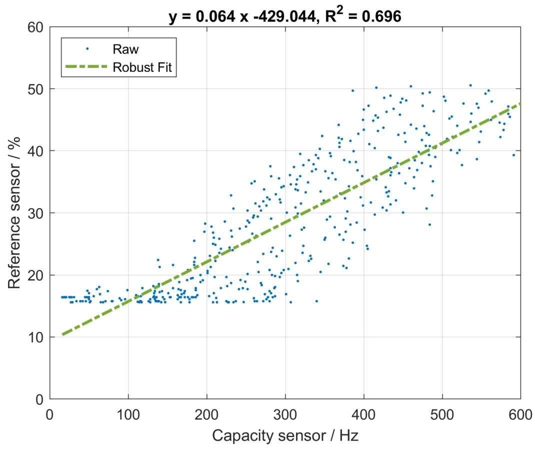


**(b)** Second measurement cycle.

**Fig. 5:** Developed sensor signal in Hz vs. reference sensor in %: Correlation between the developed and the reference sensor for the 0–50 % ice thickness range.

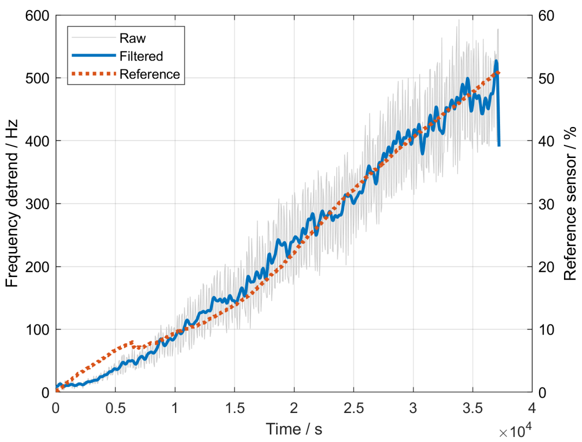


**(a)** First cycle data filtered.

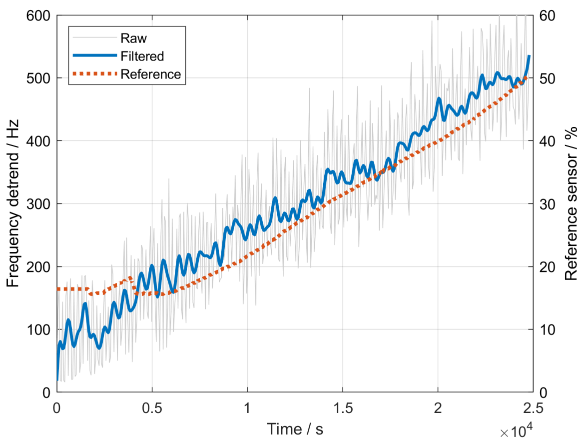


**(b)** Second cycle data filtered.

**Fig. 6:** Raw (gray) and Butterworth-filtered signals from the developed sensor in Hz s. reference sensor in %. Both covering the range of 0–50 %.

correlation plots and filtered sensor signals are presented in Figure 7 and Figure 8. In the first case, a substantially lower scatter of the measured data is observed, resulting in a high coefficient of determination of approximately $R^2 = 0.93$ (see Figure 7a). This improvement is also evident from the comparison between the raw and Butterworth-filtered signals shown in Figure 7b. A particularly strong agreement between the developed sensor and the reference sensor is found within the ice fraction range of approximately 40–80 %, corresponding to a frequency range of about 200–450 Hz. Furthermore, a measurement cycle covering the upper ice fraction range is shown in Figure 8. During this experiment, the ice thickness increased from approximately 80 % to nearly 100 % of the register. The resulting correlation, presented in Figure 8a, demonstrates a similarly strong agreement between the developed and commercial sensors, with a coefficient of determination of approximately $R^2 = 0.94$. In addition, the frequency signal exhibits considerably lower noise levels than in the previously discussed measurements. A good correspondence between both sensors can be observed in the frequency range between approximately 450 and 750 Hz, as shown in Figure 8b. These results indicate that the developed capacitance sensor is capable of reliably tracking ice growth over the entire range of ice thickness as the commercial one, particularly when the signal-to-noise ratio is favorable.

In addition to the active charging periods, sensor data were recorded during the inactive thawing phases, when the process thermostat was switched off during nights and weekends. Two representative examples of the sensor response during melting are shown in Figure 9. In Figure 9a, the reduction in ice fraction from approximately 12 % to 6 % is presented, while Figure 9b illustrates a melting process from approximately 50 % to 40 % ice fraction. The lower ice fraction case required approximately twice the time to reach the same relative change

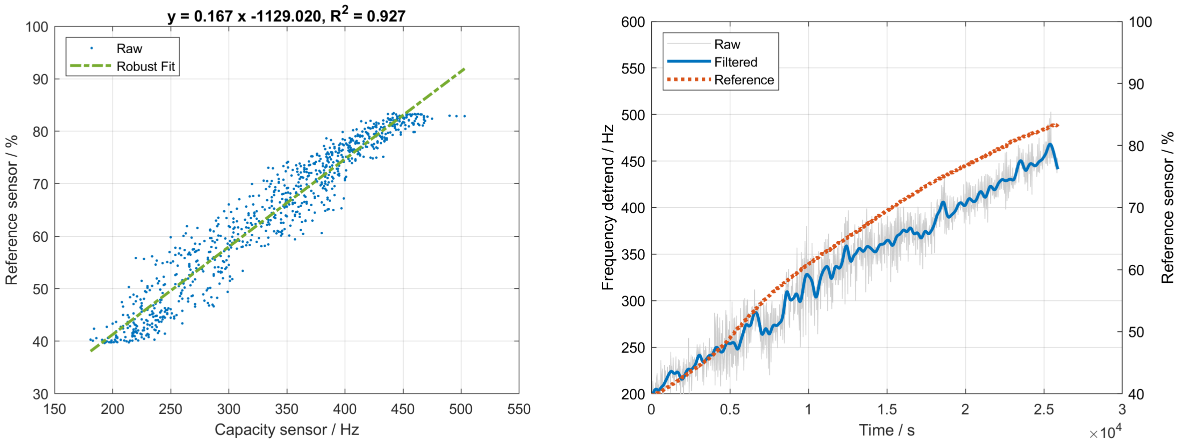


**(a)** Correlation data.

**(b)** Filtered data.

**Fig. 7:** Developed sensor signal in Hz vs. reference sensor in %: (a) Correlation between the developed and the reference sensor for the 40–80 % ice thickness range. (b) Raw and filtered signal.

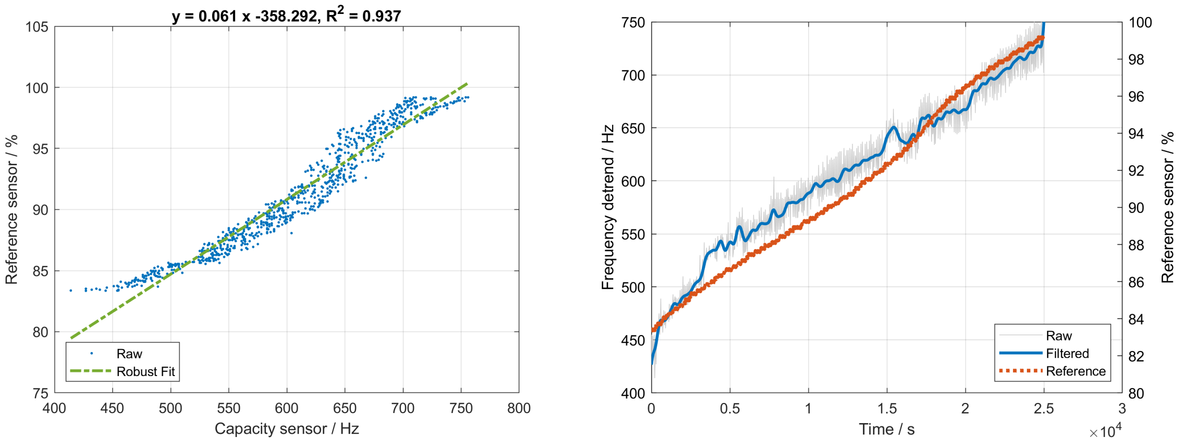


**(a)** Correlation data.

**(b)** Filtered data.

**Fig. 8:** Developed sensor signal in Hz vs. reference sensor in %: (a) Correlation between the developed and the reference sensor for the 80–100 % ice thickness range. (b) Raw and filtered signal.

in ice thickness. This behavior can be attributed to the reduced heat transfer in the later stages of melting, as only a limited heat exchange area remains in contact with the ice. Despite the slow and gradual change in ice thickness, the developed capacitance sensor is able to continuously track the melting process and exhibits good agreement with the commercial reference sensor. These results demonstrate that the sensor is capable of monitoring not only ice formation during charging but also ice loss during extended standby periods.

Evaluating the performance of the developed capacitance sensor across multiple measurement cycles is challenging. The gradual increase of the sensor frequency was observed during extended operation. This behavior is attributed to a combination of temperature-dependent dielectric properties of water, thermal drift of the measurement electronics, and dielectric polarization effects. Future work will therefore focus on temperature compensation and long-term stability investigations of the sensor system. Ideally, an offset and calibration measurement should be performed prior to each experiment. However, this is difficult to implement in practice due to the long duration of the charging cycles, the limited available operating time during working days, and the time-sensitive nature of the freezing and melting processes. To provide a clearer visualization of the sensor behavior, several charging cycles were therefore combined and arranged on a continuous timeline, as shown in Figure 10. For clarity, nighttime periods, inactive phases, and preparation steps were removed, and only the periods exhibiting a positive ice accumulation trend are shown. Although small offsets between consecutive days remain visible and the transition from one measurement day to the next does not always align perfectly (see Figure 10a), the overall trend of ice growth is clearly reproduced by the developed sensor. In particular, the agreement with the reference sensor is maintained over multiple days and charging cycles. Furthermore,

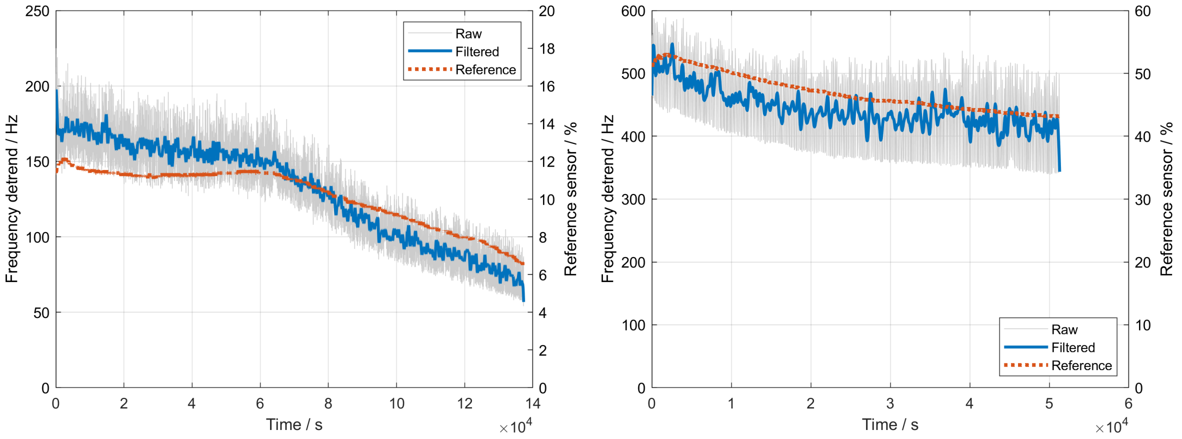


**(a)** End of inactive melting process.

**(b)** In the midst of inactive melting.

**Fig. 9:** Examples of inactive melting shown by the recorded sensor data: (a) reduction from approximately 12 % to 6 % and (b) from 50 % to 40 % ice thickness.

local deviations can be observed in some measurements. For example, in Figure 10b, the reference sensor exhibits a distinct dip at the end of Day 1. This behavior is attributed to local ice formation conditions around the sensor mounting position. Since both the reference and developed sensors are installed only at a limited number of locations along the HEX register, the local ice growth may not be perfectly uniform. In some cases, the expanding ice layer can exert mechanical forces on the sensor cable, causing slight displacement and consequently small deviations in the measured signal. Despite these effects, the developed capacitance sensor reliably captures the overall ice accumulation trend throughout the investigated measurement period.

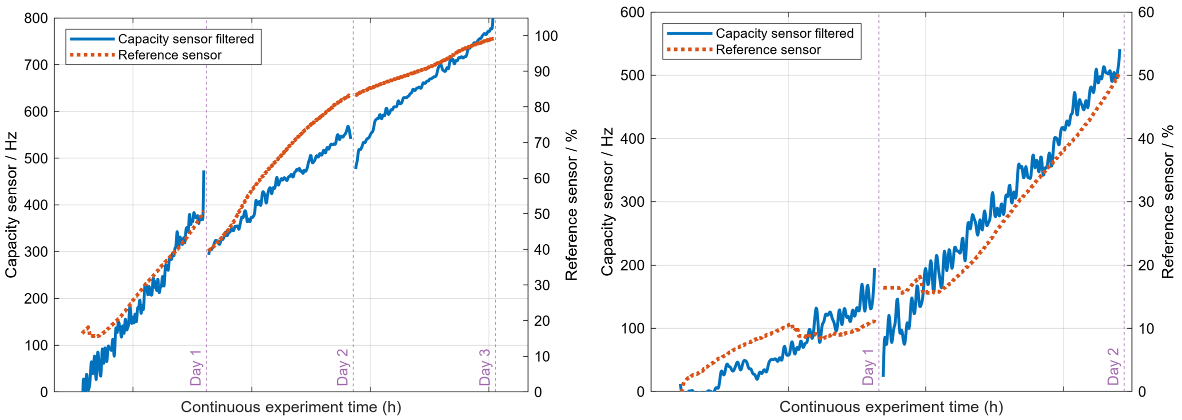


**(a)** 0 to 100% in 3 days.

**(b)** 0 to 50% in 2 days.

**Fig. 10:** Multiple measurement cycles visualized as continuous timeline. (a) Full range of ice formation over 3 days and (b) 2 days of formation up to 50 %.

## 4. Conclusion and Outlook

A low-cost capacitive sensor for monitoring the state of charge (SOC) of an ice storage system was successfully developed and validated. The sensor was designed using commercially available electronic components and demonstrated reliable operation under real application conditions. Validation against a reference sensor showed a good correlation over multiple charging and discharging cycles, confirming the capability of the proposed approach to track ice growth and melting processes within the storage. The main findings of this work are summarized as follows:

- A frequency-based capacitive sensor was successfully developed for ice thickness and SOC monitoring.
- The sensor can be manufactured at low cost using simple electronic components.

- Validation under realistic operating conditions in a 1.25 $m^3$ ice storage system demonstrated a good agreement with a commercial reference sensor.
- The developed method enables an SOC determination concept analogous to that used for electrical batteries by relating the measured capacitance change to the geometrical properties of the HEX and storage system.
- Due to the low manufacturing cost, multiple sensors can be distributed throughout a storage tank, enabling improved spatial resolution and potentially more accurate SOC predictions.

Although the results demonstrate the feasibility of the proposed approach, several aspects require further investigation. A temperature-dependent drift and measurement noise were identified, highlighting the need for a more detailed understanding of the underlying noise sources and their decoupling. Future work will therefore focus on optimizing the sensor design and evaluating the influence of different sensor parameters, including cable length, positioning, and geometric configurations. Furthermore, complementary optical sensors are currently being investigated as safety and alarm sensors for detecting the formation of continuous ice bridges between neighboring HEX tubes. A proof of concept for this approach has already been demonstrated in previous work, and long-term validation measurements are currently underway. Overall, the presented results indicate that capacitive sensing is a promising and economically attractive approach for distributed monitoring of ice storage systems and may contribute to improved control, operation, and performance assessment of latent thermal energy storage technologies.

*Acknowledgment*

This work has been supported by the Government of Upper Austria in the project 'COMPESTO – comprehensive energy storage', Research Grant Wi-2022 – 600132/7-Au and in the project 'ICE4H&C – ICE Heating and Cooling for SFH and MFH' (FET-Future energy technologies call).

## References

S. S. M. Ajarostaghi, S. Poncet, K. Sedighi, and M. A. Delavar. Numerical modeling of the melting process in a shell and coil tube ice storage system for air-conditioning application. *Applied Sciences*, 9(13):2726, 2019. doi: 10.3390/app9132726.

V. G. Artemov and A. A. Volkov. Water and ice dielectric spectra scaling at 0°c. *Ferroelectrics*, 466(1): 158–165, 2014. doi: 10.1080/00150193.2014.895216.

R. P. Auty and R. H. Cole. Dielectric properties of ice and solid d2o. *The Journal of Chemical Physics*, 20(8): 1309–1314, Aug. 1952. ISSN 1089-7690. doi: 10.1063/1.1700726.

T. Barz, D. Seliger, K. Marx, A. Sommer, S. F. Walter, H. G. Bock, and S. Körkel. State and state of charge estimation for a latent heat storage. *Control Engineering Practice*, 72:151–166, Mar. 2018. ISSN 0967-0661. doi: 10.1016/j.conengprac.2017.11.006.

H. Bastida, I. de La Cruz-Loredo, and C. E. Ugalde-Loo. Effective estimation of the state-of-charge of latent heat thermal energy storage for heating and cooling systems using non-linear state observers. *Applied Energy*, 331:120448, 2023. doi: 10.1016/j.apenergy.2022.120448.

D. Carbonell, D. Philippen, M. Y. Haller, and E. Frank. Development and validation of a mathematical model for ice storages with heat exchangers that can be de-iced. *Energy Procedia*, 57:2342–2351, 2014. doi: 10.1016/j.egypro.2014.10.242.

D. Carbonell, D. Philippen, M. Y. Haller, and S. Brunold. Modeling of an ice storage buried in the ground for solar heating applications. validations with one year of monitored data from a pilot plant. *Solar Energy*, 125: 398–414, 2016. doi: 10.1016/j.solener.2015.12.009.

A. Colangelo, E. Guelpa, A. Lanzini, G. Mancò, and V. Verda. Compact model of latent heat thermal storage for its integration in multi-energy systems. *Applied Sciences*, 10(24):8970, 2020. doi: 10.3390/app10248970.

Y. Dou, J. Qin, and X. Chang. The study of a capacitance sensor and its system used in measuring ice thickness, sedimentation and water level of a reservoir. In *2009 International Forum on Information Technology and Applications*, pages 616–619, Chengdu, China, 2009.

D. C. Elton. The origin of the debye relaxation in liquid water and fitting the high frequency excess response. *Physical Chemistry Chemical Physics*, 19(28):18739–18749, 2017. ISSN 1463-9084. doi: 10.1039/c7cp02884a.

M. A. Ezan, L. Cetin, and A. Erek. Ice thickness measurement method for thermal energy storage unit. *Journal of Thermal Science and Technology*, 31(1):1–10, 2011.

G. Issayan, P. Kefer, C. Wagner, E. Mehmedovski, and B. Zettl. State of charge determination of an ice storage by optical sensors. 2025. URL `https://icenss2025.sciencesconf.org/`. International Conference of Energy Storage and Saving ; Conference date: 26-05-2025 Through 28-05-2025.

J. P. Leitzke, T. Mitterer, and H. Zangl. Capacitive sensing of icing under vacuum and cryogenic temperatures. *Sensors*, 19(16):3574, Aug. 2019. ISSN 1424-8220. doi: 10.3390/s19163574.

C. Li, J. Hou, Y. Wang, S. Wei, P. Zhou, Z. He, Y. Wang, H. Zhang, and S. You. Dynamic heat transfer characteristics of ice storage in smooth-tube and corrugated-tube heat exchangers. *Applied Thermal Engineering*, 223:120037, 2023.

S. Mancin and M. Noro. Reversible heat pump coupled with ground ice storage for annual air conditioning: An energy analysis. *Energies*, 13(23):6182, 2020. doi: 10.3390/en13236182.

T. Mehmood, N. U. H. Shah, M. Ali, P. H. Biwole, and N. A. Sheikh. Simplified mathematical model and experimental analysis of latent thermal energy storage for concentrated solar power plants. *Journal of Energy Storage*, 41:102871, 2021. doi: 10.1016/j.est.2021.102871.

S. Sibilia, L. Tari, F. Bertocchi, S. Chiodini, and A. Maffucci. A capacitive ice-sensor based on graphene nano-platelets strips. *Sensors*, 23(24):9877, Dec. 2023. ISSN 1424-8220. doi: 10.3390/s23249877.

G. Steinmaurer, M. Krupa, and P. Kefer. Development of sensors for measuring the enthalpy of pcm storage systems. *Energy Procedia*, 48:440–446, 2014. ISSN 1876-6102. doi: 10.1016/j.egypro.2014.02.052.

J. Vivian, P. Heer, and M. Fiorentini. Optimal sizing and operation of seasonal ice thermal storage systems. *Energy and Buildings*, 300:113633, 2023. doi: 10.1016/j.enbuild.2023.113633.

A. A. Volkov and A. A. Vasin. Dielectric properties of water and ice: A unified treatment. *Ferroelectrics*, 538 (1):83–88, 2019. doi: 10.1080/00150193.2019.1569989.

C. Wagner and G. Issayan. Modelling and experimental characterization of ice storage for state of charge determination. *Environmental and Climate Technologies*, 29(1):784–796, Jan. 2025. ISSN 2255-8837. doi: 10.2478/rtuect-2025-0052.

J. Wilson, R. J. Barthorpe, and F. Terzioglu. Alternative sensing for state-of-charge estimation of latent heat thermal energy storage. *Energies*, 18(11):2853, May 2025. ISSN 1996-1073. doi: 10.3390/en18112853.

X. Zhi, H. Cho, B. Wang, C. Ahn, H. Moon, and J. Go. Development of a capacitive ice sensor to measure ice growth in real time. *Sensors*, 15(3):6688–6698, Mar. 2015. ISSN 1424-8220. doi: 10.3390/s150306688.

G. Zsembinszki, C. Orozco, J. Gasia, T. Barz, J. Emhofer, and L. F. Cabeza. Evaluation of the state of charge of a solid/liquid phase change material in a thermal energy storage tank. *Energies*, 13(6):1425, Mar. 2020. ISSN 1996-1073. doi: 10.3390/en13061425.